Optical properties of DNA-hosted silver clusters

Markesevic, N.

CHAPTER 3

Polarization resolved measurements of individual DNA-stabilized silver clusters

Polarization resolved excitation and emission measurements on individual 10-15 atom silver clusters formed on DNA are presented. The emission is highly linearly polarized, typically around 90% for all emitters, whereas the polarization dependence of the excitation strongly varies from emitter to emitter. These observations support the hypothesis that the luminescence arises from collective electron oscillations along rod-shaped silver clusters, whereas the excitation process does not necessarily have a strong preferential polarization direction and thus may involve energy and/or charge transfer between the cluster and DNA. In addition to stabilizing the clusters, the DNA also appears to strongly influence the available paths for excitation.

This Chapter is based on: N. Markešević, S. S. R. Oemrawsingh, D. Schultz, E. G. Gwinn, D. Bouwmeester, *Polarization resolved measurements of individual DNA-stabilized silver clusters*, Adv. Optical Mater. **2**, 765 (2014).

3.1 Introduction

Advances in DNA nanotechnology and separation science have recently enabled the isolation of DNA-stabilized clusters of silver at the size scale of 10 to 24 silver atoms [53, 76]. Because these small clusters can be fluorescent [10], with high quantum yields, and because the specific DNA sequence strongly influences the optical properties of the stabilized clusters, these Ag:DNAs are beginning to be intensively studied for applications in sensing [16] and biolabeling [17]. Such silver "nanoclusters", with just tens of metal atoms, are in a different size regime from metal nanoparticles of several to tens of nanometers dimensions that are the focus of current nanoplasmonics research [1, 2, 77]. Thus, beyond their current uses as biolabels and sensors, metal nanoclusters that are stabilized by such a versatile ligand as DNA, which itself can assemble into elaborate nanoscale shapes [23], have the potential to realize metal-organic hybrid materials at truly nanoscale dimensions, enabling functionality at enormously high spatial densities [33, 78]. Given their nanometer size scale, such cluster-based materials may also combine desirable properties usually associated with the molecular regime, such as high fluorescence quantum yields and large Stokes shifts, with emergent near-field interactions arising from the polarizability of free electron systems, as currently exploited in Surface-enhanced Raman Spectroscopy (SERS) [79], and plasmonic coupling schemes with metal nanoparticles [78].

Despite the numerous Ag:DNA [13, 17, 20, 51, 52, 65, 80] studies, little is known about the mechanism by which fluorescent excitation and emission occur. It was previously established in the literature on small metal clusters that the excitation energies are considerably up-shifted from the particle-in-box energies, due to Coulomb interactions that lead to collective, phased oscillation of the clusters valence electrons [72, 81]. Recent experimental works [19, 21] indicate that fluorescent Ag:DNA contains a neutral silver core that is surrounded by base-bound silver ions. This arrangement is analogous to the known structure of gold clusters that are stabilized by small organic ligand molecules [4, 82, 83], which possess both transitions associated with the gold core, and transitions involving charge transfer between the gold core and the surrounding ligands plus their directly attached gold atoms [82, 83]. For Ag:DNAs, the specific mode of cluster-DNA binding is unknown, but given the existence of a neutral silver core one might expect both core-centered tran-

sitions and charge transfer transitions between the core and base-attached silver ions.

In the case of such silver core-ligand transitions, small variations in the specific conformation of the DNA might be expected to affect directions of transition dipole moments. Thus it is of great interest to study individual Ag:DNAs under conditions that minimize environmental fluctuations, using techniques that can probe such orientational effects.

In this Chapter, we present single-cluster optical studies of Ag:DNAs that investigate both their response as a function of the polarization of the excitation light and the polarization of the light they emit. Single particle polarization studies have previously been used to investigate individual fluorescent molecules, providing insight into the orientation of the emitters in the surrounding medium [84, 85] as well as photophysical events of single molecules, such as rotational jumps of a single dipole, transitions into a dark state (reversible and irreversible photobleaching) and spectral jumps [86]. Another example of the strength of polarization resolved measurements is the study of Au_{25} nanoclusters stabilized by bovine serum albumin (BSA) [5]. Such experiments have also been carried out on much larger, individual metal nanoparticles, revealing the strong dependence of polarization response on shape [3].

We will use conventional far-field polarization imaging in which the detected dipole is projected onto the imaging plane. A polarization rotator controls the polarization of the excitation light, and the emission is collected after passing through a polarizer. This technique determines the sensitivity of the emission to the polarization of the excitation light together with the polarization of the emission. A tilt of an individual Ag:DNA out of the imaging plane will only reduce the detection intensities without affecting the polarization modulation depths [87].

Here we focus on two distinct Ag:DNA emitters. Emitter A is a silver cluster stabilized by a native DNA hairpin strand with 6 bases in the loop and 4 base pairs in the stem. Emitter B is a silver cluster stabilized by 28 base long DNA strand. These emitters produce relatively stable and bright fluorescence following excitation within the spectral range of a ring dye laser (see section 3.4 for details).

3.2 Results and discussion

The focus of this work will mainly pertain to linear polarization properties. We will show that the emission of Ag:DNAs is nearly completely linearly polarized, whereas the polarization of the absorbed light largely varies from emitter to emitter. While the linearly polarized emission of the Ag:DNAs is consistent with collective electronic oscillations along the longitudinal axis of a rod, the emitter-dependent excitation polarization behavior implies the importance of the DNA environment of the Ag cluster in the absorption process.

For a given set of excitation and detection polarizations, we obtain a number of bright spots on the CCD camera (Figure 3.1 a). Most spots are circularly symmetric and diffraction limited. Furthermore the maxima of the emission from different spots have comparable intensities but occur at different polarization settings. These features indicate that we are observing an ensemble of individual optical emitters. A small number of spots, approximately 5%, have very different properties; in particular they are significantly brighter, show hardly any polarization dependence, and have sometimes an asymmetric shape. These emission properties are typical for small clumps of multiple emitters and of certain fluorescent impurities, and therefore we exclude them from our study of individual emitters.

To determine the intensity of each individual emitter, we first select a rectangular area, typically 30 by 30 pixels, approximately 10 times as large as diffraction limited spot, containing an emitter (Figure 3.1 a). Taking the pixel with the maximum number of counts as the center of the Gaussian, it can be plotted as a function of radius (Figure 3.1 b), and fitted according to:

$$f = a + b \cdot exp(-x^2/\sigma^2), \tag{3.1}$$

where a is a constant offset representing background fluorescence, b describes the height of the Gaussian, and σ is the width which is set by the point spread function of the optical system.

The detected intensity I of an emitter (which is in general a function of the angle between the excitation and detection polarization and of the orientation of the Ag:DNA) is then proportional to the volume of the Gaussian term in Eq. 3.1. Since the spots are diffraction limited σ should be mainly determined by the optical imaging system, not by the properties of the emitter.

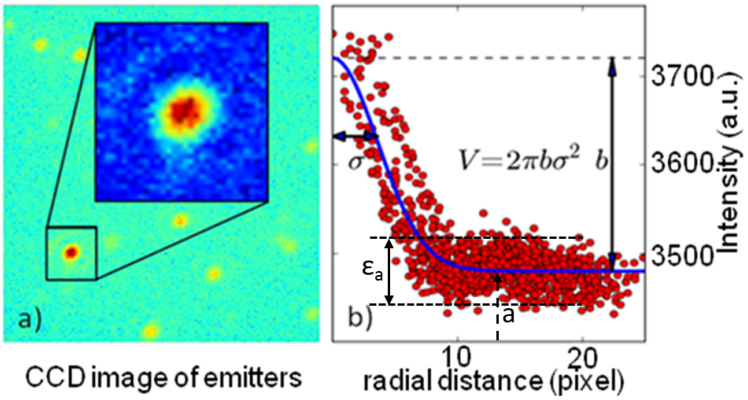

Figure 3.1: DNA:Ag emitters observed by a cooled CCD camera. The intensity per emitter is determined by selecting a rectangular area around the emitter (a), and fitting a cylindrical Gaussian function with a constant offset to the pixel intensity as a function of distance from the intensity maximum, which is the position of the emitter (b). From the fitted parameters, we calculate the emitter intensity. ε_a represents the noise floor of the measurements.

Indeed, this fitting parameter turns out to have approximately the same value for emitters when measured near the optimal polarization settings. Therefore the integral of the exponent in Eq. 3.1 can be approximated by a constant, and the measured intensity I, becomes proportional to b. In order to determine the error bars on a given data point we perform an error propagation using the full covariance matrix based on the fitting parameters b and σ. Applying the same procedure to each image, for each set of excitation and emission polarization angles (361 images in total), allows us to produce a contour plot, where the emitter intensity (color scale) is given as a function of the excitation, θ_{ex}, and emission, θ_{em} , polarization angles (Figure 3.2).

In order to extract polarization modulation characteristics of the emission process, we consider the intensity of the emitter as a function of excitation (emission) polarization angle, for a fixed emission (excitation) angle. The vertical and horizontal slices of the contour graph in Figure 3.2 b, c show examples. For each slice, we fit the modulation depth, M, and a scaling factor, N, using the following relation:

$$I(\theta) = N(1 + M\cos(2(\theta - \phi))), \tag{3.2}$$

Here, θ is the fixed emission (or excitation) polarization angle and Φ is the (random) orientation angle that the Ag:DNA makes with the polarization axes. Thus we extract a modulation depth, M, for each fixed polarization angle, θ. Applying the same procedure to cross-sections 10° apart, we find the modulation depth of the emitter, $< M_{em} >$, and the orientation angle, $< \Phi_{em} >$ as the error-weighted averages over all angles for which there was sufficient signal.

We note that the typical offset, a, as extracted from fitting graphs like the one presented in Figure 3.1 b is an order of magnitude larger than b, indicating a significant background emission. The noise level of this background emission is indicated as ε_a in Figure 3.1 b. For polarization settings at which a specific emitter is near its minimal emission, b becomes comparable to, or smaller than ε_a, and the fit becomes unreliable. Those data points are indicated as blue points in graphs d)-g) and are omitted in determining $< M >$ and $< \Phi >$.

To place the results shown in Figure 3.2 within a broader context, we discuss results of prior polarization measurements on individual dye molecules and metal nanoparticles. For individual fluorescent dye molecules, polarization measurements are limited to highly photostable dyes that permit collection of many photons before bleaching. [86] The dependence of the emission intensity, I, from a single molecule on the excitation polarization angle, θ_{ex}, probes the orientation of the molecule's absorption dipole moment, μ_{ex}. The dependence on the angle of emission polarizer, θ_{em}, probes the orientation of the molecule's emission dipole moment, μ_{em}.

Single molecule polarization studies on various dye molecules have found the same functional dependence on both angles, θ_{ex} or θ_{em}, given by Eq. 3.2. In principle, the molecular orientation, described by Φ, can differ for excitation and emission if the molecule undergoes orientational reorganization within the fluorescence lifetime. As long as emission is from the same electronic manifold as that of the initial excited state, such effects are typically small: the largest quantified shift in single molecule orientation was $\sim 5\%$, for Cy5. Regardless, for single molecular fluorophores the modulation depth M is unity for excitation and for emission, corresponding to ideal dipole behavior in both cases [86, 88].

In contrast, the polarization modulation depth for metal nanoparticles, much larger in size than the few atom silver clusters addressed in this

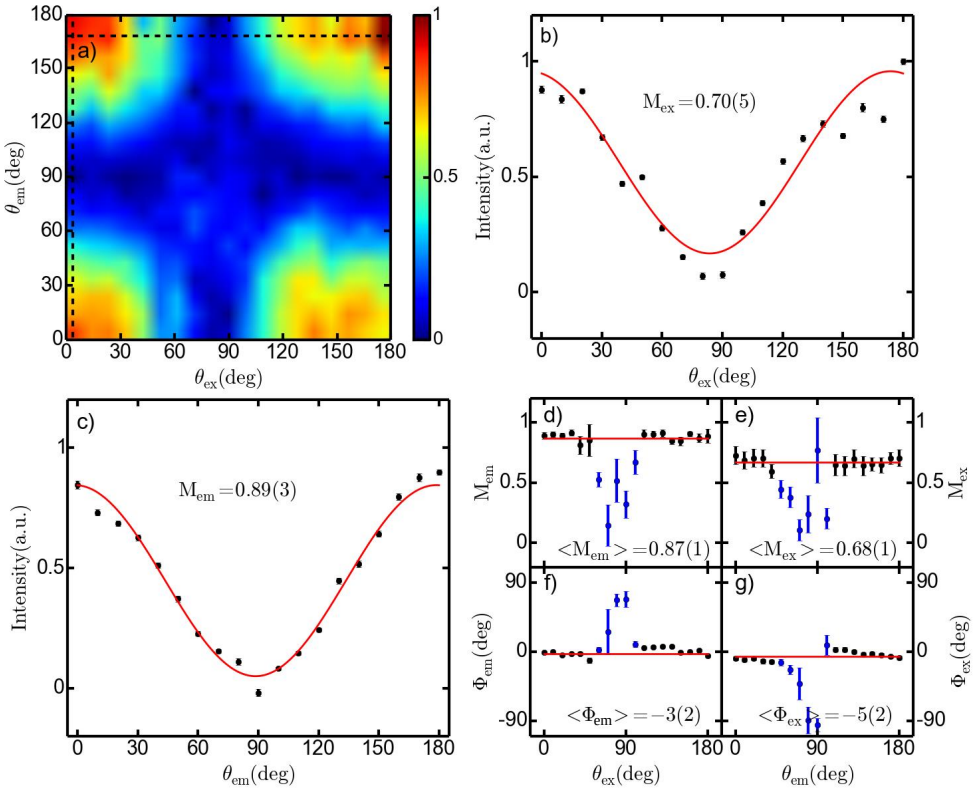

Figure 3.2: Polarization measurement of a single emitter. a) Intensity (color scale) of the emitter is presented as a function of excitation, θ_{ex}, and emission polarization angles, θ_{em}. Each of the cross-sections at constant excitation or emission polarization angle (vertical and horizontal) is fitted with the expected dependence for an ellipsoidal cluster (in the text) from which we obtain modulation depth, M, and phase, Φ. b) Cross-section for $\theta_{em} = 170°$ gives $M_{ex} = 0.70(5)$. c) Cross-section for θ_{ex}=0° gives $M_{em} = 0.89(3)$. d) Averaged emission modulation depth and e) averaged phase of the emitter are extracted from an error weighted linear fit (red line) of the data points from the cross-section fits. f) Averaged excitation modulation depth and g) averaged phase are found similarly as for d) and e). Cross-sections for which the intensity of the emitter is smaller than, or equally to the noise floor ε_a, (see Figure 1b) are indicated as blue regions in (a). As explained in the text, data points extracted from those cross-sections (blue data points in 2d-g) are not reliable and are therefore excluded in determining the average modulation depth $< M >$.

work, varies widely with a strong dependence on the specific nanoparticle shape [3]. Since the fluorescence quantum yields of metal nanoparticles are very small ($\sim$ 0.001% or less) [2, 89], most polarization measurements have focused on determining the single nanoparticle extinction as a function of the polarization, θ_{ex}, of the excitation light, using techniques such as photothermal imaging [90], light scattering microscopy [91], and extinction microscopy [92]. The intensity dependence on θ_{ex} has the same overall sinusoidal form as for individual molecules (Eq. 3.2). The modulation depth M vanishes for perfectly spherical particles, because any polarization angle gives the same excitation rate of the collective, plasmonic mode of the free electrons. For real nanoparticles with slight deviation from perfectly spherical shapes, M is found to be $<\sim 0.1$ [3].

In the case of rod-shaped or ellipsoidal metal nanoparticles, the polarization response is quite different from that of spherical particles [3]. The anisotropic shape results in more than one collective excitation: a low-energy longitudinal mode and a higher energy transverse mode [83]. The development of sensitive photothermal imaging techniques has enabled direct measurement of the dependence of the absorbance of gold nanorods on excitation polarization, for rods with dimensions of $\sim$ 25 nm x 75 nm, corresponding to $\sim 10^6$ Au atoms [89]. For these nanorods, single particle measurements at the energy of the longitudinal mode find modulation indexes M very close to 1 for rods with aspect ratios (length to diameter) of ~ 3, while measurements at the energy of the transverse mode find $M << 1$. Thus, at energies near the longitudinal mode, the polarization dependence of the absorbance again has the ideal dipolar form.

Based on these prior studies, we would expect that if silver nanoclusters behaved like single dye molecules, the fluorescence intensity would exhibit $M = 1$ for both excitation and emission. If instead they behaved as nearly spherical nanoparticles, the fluorescence intensity should exhibit $M << 1$, as a function of both θ_{ex} and θ_{em}. On the other hand, for rod-shaped nanoparticles near the longitudinal resonance, the fluorescence intensity should exhibit $M = 1$ as a function of both θ_{ex} and θ_{em}. Figure 3.2 shows that for an Ag:DNA emitter of type B, we obtained $< M_{ex} >= 0.70(5)$ and $< M_{em} >= 0.89(3)$. Other individual emitters of both types B and A that were photostable enough to enable a collection of the full two-dimensional polarization scan also showed similar characteristics. However, because the

two-dimensional raster scan of θ_{ex} and θ_{em} in Figure 3.2 a requires long exposure times, approximately 1 hour, most emitters photobleach before the full contour map can be collected. The full contour plot has some redundancy of information for determining the excitation and emission modulation. We removed this redundancy, thereby decreasing the measurement time and enabling the study of a larger population of emitters, in the following way. To determine the excitation modulation depth, for each individual emitter we collect all emission while varying the excitation polarization angle. To determine the emission modulation depth, we excite emitters using right circularly polarized light, while varying the emission polarization angle. In order to check that the emission modulation $< M_{em} >$ is independent of the excitation polarization, we performed additional measurements using linear and circularly polarized excitation light and confirmed that there is no significant modulation dependence on the excitation polarization.

For individual emitters we extracted the excitation and emission modulation depths. Figures 3.3 a, b show the results for type A emitters. From the obtained statistics and the scattered values of excitation modulation depth, we can conclude that the excitation properties vary significantly amongst emitters. This variation can be rationalized by considering that the DNA may adopt a range of conformations relative to the clusters. Even at low temperatures, small changes in conformation of the polymer-like DNA strand around an individual cluster may occur over the timescale of the experimental measurement. To the extent that the DNA affects the excitation of the cluster, for example by energy or charge transfer processes, such conformational variation could produce fluctuations in the excitation moment orientation, resulting in a lowered excitation modulation depth on the time-average. Variation in the details of the average DNA conformation from emitter to emitter could then account for the wide spread in excitation modulation depths evident in both Figure 3.3 a (type A emitters) and Figure 3.3 c (type B emitters). This picture can give a plausible explanation for an excitation modulation depth significantly different from the value of 1.0 expected for an ideal dipole.

Comparing our polarization resolved data with the results from reference [5] on BSA-stabilized Au_{25} nanoclusters, we come to the conclusion that the systems are quite different. For the stabilized Au_{25} clusters, absorbance spectra spread broadly across the UV-visible and the excitation polarization anisotropy depends on excitation wavelength. For the DNA-stabilized sil-

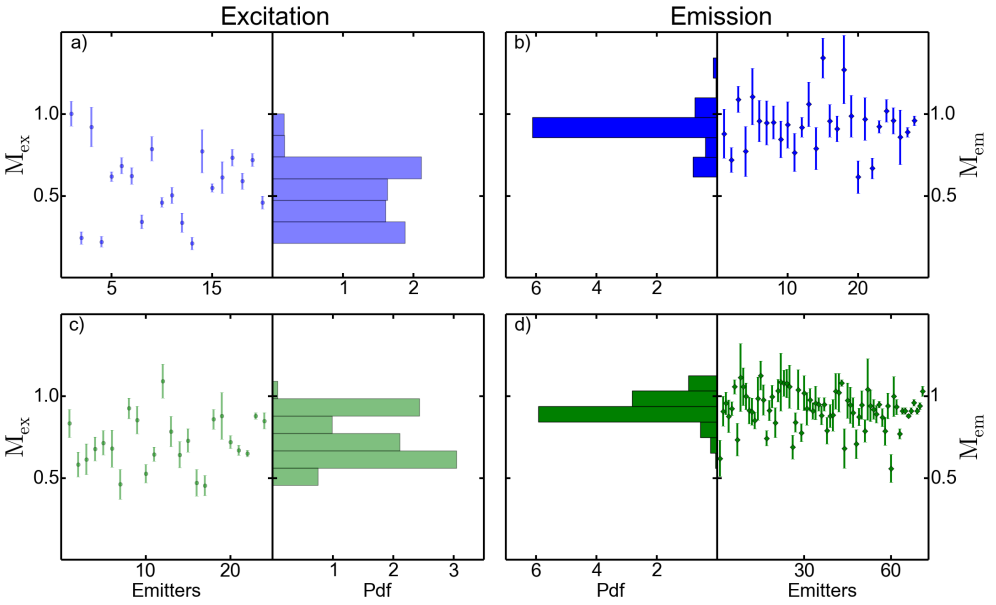

Figure 3.3: Modulation depth of Ag:DNAs of type A (blue) and B (green). Histograms of excitation modulation depth values for 20 emitters of type A (a) and 24 emitters of type B (c) show scattered values. On the other hand, the emission modulation depths for 28 emitters of type A (b) and 71 emitters of type B (d) clearly show peaks centered around 0.92 and 0.88 for types A and B, respectively. The value of the probability density function (Pdf) is normalized, such that the integral over the range is equal to one.

ver clusters, pure solutions exhibit a single, narrow peak in the absorbance at an energy that depends on cluster size [53]. Corresponding to this qualitative spectral difference from BSA-Au_{25}, our single emitter polarization measurements on Ag:DNA found no dependence on the excitation wavelength (within the tunable range of our laser, 575-595 nm). These marked differences in behavior may arise from the smaller $s - d$ splitting in gold, which produces more complex optical properties in Au relative to Ag clusters due to mixing of d and s orbital transitions in the former [22].

In striking contrast to the excitation modulation depth, Figures 3.3 b and 3.3 d show that emission modulation depth values are close to unity, the ideal dipole limit, for both types A and B emitters. Apparently the additional degrees of freedom that result in widely spread, and overall lower, excita-

tion modulation depths have much less effect on emission polarization. It seems that the emission path is much better defined, consistent with a longitudinal collective electronic mode along the cluster, as suggested in previous work [89].

Single emitter studies of the MEH-PPV heptamer also showed highly polarized emission but not excitation, similar to the Ag:DNA, but with more broadly distributed excitation modulation depths [93, 94]. For this molecular chain the polarization properties were explained by considering that excitation can take place anywhere along the generally bent chain, but the emission is only coming from a small, approximately straight, section where the optically generated electron-hole pairs will be trapped and recombine.

In the case of the Ag:DNA we expect that both the absorption and emission are localized within a relatively small region that holds the few atom silver cluster since the silver is essential for both the absorption and emission. Together with the typical shift of ~ 60nm between the excitation and emission wavelengths, this suggests that the excitation involves energy and/or charge transfer to the Ag cations and/or host DNA that support the central silver cluster. The excitation is therefore only partially linearly polarized along the axis of the cluster. The small metallic cluster is likely to act as an antenna that enhances the incoming optical field, thereby enhancing the absorption probability in its direct vicinity. The excitation will rapidly decay due to the numerous degrees of freedom in the complex system to an electronic excitation within the central silver atoms. Modeling the emitter as a several-atoms long silver rod with conducting electrons gives reasonable agreement with the observed emission wavelength [22].

3.3 Conclusion

We have measured the polarization-dependent excitation and emission properties of single Ag:DNA emitters. Measurements on many individuals of two different types of emitters at 1.7 K reveal a large emission modulation depth, indicating that these small clusters have properties similar to noble metal nanorods, typically containing millions of atoms. For comparison, the typical emission modulation depths of ~ 0.9 that we find for fluorescent silver clusters would correspond to a length to diameter aspect ratio of $> 1.6 : 1$ in the limit of much larger silver nanoparticle rods [95]. On the other hand, the

disperse values for excitation modulation depth indicate that the excitation pathways differ from those for emission. Thus we ascribe the luminescence mechanism to the collective electron oscillations, while the excitation may involve energy and/or charge transfer between the cluster and DNA. The improved characterization of the optical properties of the individual Ag:DNA emitters provides qualitative insight in the optical processes and valuable input for the quantum mechanical modeling of these complex structures.

Furthermore, it also provides information on how to construct more elaborate patterns containing many interacting emitters with aligned dipole moments. The above findings are likely to apply to all DNA-encapsulated noble metal clusters. The DNA molecule is likely not only a stabilizing agent, but may also actively participate in the excitation process. Our polarization microscopy studies reveal behavior of DNA-stabilized silver nanoclusters that differs in distinctive ways from the characteristic behaviors of both the molecular and metal nanoparticle regimes. Thus, novel photophysics is emerging from metal clusters with $\sim$ 1nm size scales, held within a DNA environment.

3.4 Experimental methods

Synthesis of fluorescent Ag:DNA clusters: Samples were prepared by mixing oligonucleotide (IDT, standard desalting) with ammonium acetate (99.999%, Sigma Aldrich) and $AgNO_3$ (99.9999%, Sigma Aldrich). After 20 minutes of incubation, a reducing agent $NaBH_4$ (99%, Sigma Aldrich) was added to the solution, producing fluorescent emitters. The emitter A is stabilized by a native DNA hairpin (5-CCG-CCA-CCC-CGC-GGT-3), containing 5 Cytosines (C) and 1 Adenine (A) in the loop and four base pairs in the stem. It was used without further purification. Final concentrations are: (50 μM) DNA, (350 μM) $AgNO_3$, (100 μM) $NaBH_4$, and (20 mM) ammonium acetate.

The second emitter, B, is stabilized by a 28 base long DNA strand (5-CAC-CGC-TTT-TGC-CTT-TTG-GGG-ACG-GAT-A-3). Final concentrations are: (5 μM) DNA, (50 μM) $AgNO_3$, (25 μM) $NaBH_4$, and (10 mM) ammonium acetate. Emitter B was HPLC purified using a Waters 2695 Separations Module with autoinjector and a Waters 2487 Dual Wavelength absorbance detector (10 μL volume), set to monitor the visible peak of each silver cluster. Separations used linear gradients from 15% to 35% of B (35 mM TEAA/MeOH) with A (35 mM TEAA/H_2O) on a 50 mm 4.6 mm Kinetex C18 core shell col-

umn with 2.6 μm particle size and 100 Å pore size (Phenomenex). Following HPLC purification, samples were dialyzed overnight into (50 mM) ammonium acetate using 10 kDa MWCO MINI dialysis units (Thermo Scientific).

The composition of emitters B, 15 silver atoms on the DNA strand, was identified previously by mass spectrometry of the pure material [19]. Based on the established correlation between the silver content and the excitation/emission properties, the number of silver atoms in emitter A is similar.

Characterization method: Samples were diluted in 5 mg/ml poly(vinyl alcohol) (PVA) and spin-cast onto a fused silica substrate. In order to suppress blinking and increase signal to noise ratio, all the measurements were performed at 1.7 K. The samples were mounted in a custom-built helium-bath cryostat and were excited at a wavelength of 585 nm by the ring dye laser (Coherent 899) with Rhodamine 590 Tetrafluoroborate dye (Exciton). The excitation light was filtered with a short-pass filter (edge at 600 nm), while the emission path contained a band-pass filter centered at 647 nm, with a width of 57 nm. A dichroic mirror (edge at 600 nm) was used to separate the excitation and emission paths. A polarization rotator controlled polarization of the excitation, whereas the emission was collected after passing through a polarizer. In order to preserve excitation and emission polarization in our experiment, we used a 0.8 NA objective inside the cryostat for both the excitation and the collection of the emission light. Fluorescence of the emitters was detected with a cooled CCD camera (Ikon-M 934-BR-DD, Andor Technology).